Aluminium-induced nanocrystalline Ge formation at low temperatures

2007 J. Phys.: Condens. Matter 19 076206

(http://iopscience.iop.org/0953-8984/19/7/076206)

IOP PUBLISHING JOURNAL OF PHYSICS: CONDENSED MATTER

J. Phys.: Condens. Matter **19** (2007) 076206 (16pp) doi:10.1088/0953-8984/19/7/076206

Aluminium-induced nanocrystalline Ge formation at low temperatures

L R Muniz[1], C T M Ribeiro[2], A R Zanatta[2] and I Chambouleyron[1,3]

[1] Instituto de Física 'Gleb Wataghin'—UNICAMP, PO Box 6165, Campinas 13083-970, Brazil
[2] Instituto de Física de São Carlos—USP, PO Box 369, São Carlos 13560-970, Brazil

E-mail: ivanch@ifi.unicamp.br (I Chambouleyron)

Received 31 October 2006, in final form 1 November 2006
Published 2 February 2007
Online at stacks.iop.org/JPhysCM/19/076206

Abstract

The present work contributes to establishing the role of hydrogenation and of the substrates in the aluminium-induced crystallization process of amorphous germanium layers. For such a purpose, four series of a-Ge(Al) samples, deposited under identical nominal conditions, were studied: hydrogenated samples, H-free samples, and samples deposited on crystalline silicon and on glass substrates, respectively. On purpose, the impurity concentration was kept at a doping level ($10^{-5} < [\mathrm{Al/Ge}] < 2 \times 10^{-3}$). Furthermore, the films were submitted to isochronal cumulative thermal annealing in the 200–550 °C range. Raman scattering spectroscopy was used to characterize the crystallization process. The role of Al impurity as a precursor seed for the crystallization of a-Ge:H has been clearly established, confirming that the metal-induced crystallization (MIC) phenomenon occurs at an atomic level. Moreover, it has been found that hydrogenation and the periodic nature of the substrate play a fundamental role in the appearance of crystal seeds at low temperatures. The evolution of crystallization with annealing temperature and the analysis of the distribution of crystallite sizes indicate that the formation of crystal seeds occurs at the amorphous film–substrate interface. The importance of fourfold-coordinated aluminium as the embryo of nanocrystal formation is discussed.

1. Introduction

It is well established that certain metals induce the crystallization of amorphous networks at relatively low temperatures [1, 2]. The microscopic mechanism behind the effect—still a matter of debate—appears to depend on the chemical specificity of the metal and on the way it interacts with the amorphous network. The subject has fuelled an ever-increasing effort to understand the mechanisms that govern the metal-induced crystallization (MIC) process as well as the

[3] Author to whom any correspondence should be addressed.

dimensions of the resulting crystals and their orientation. The interest is not only academic, but also driven by potential applications such as, for example, the low-temperature manufacturing of micro- or nanoelectronic devices onto plastic substrates [3, 4].

In previous publications our research group reported the low-temperature crystallization of aluminium-doped hydrogenated amorphous germanium films [a-Ge:H(Al)] deposited onto crystalline silicon substrates [5–7]. The present contribution identifies the different contributions to the MIC phenomenon. In particular, we report on: (i) the role of aluminium impurity; (ii) the role of hydrogenation, (iii) the effect of film stress; and (iv) the influence of the substrate on the whole MIC process. To that aim Al-doped and Al-free, hydrogenated and H-free, a-Ge samples were deposited onto crystalline (c-) silicon and onto glass substrates. The films were annealed at increasing temperatures and their structures were investigated with Raman scattering spectroscopy after each thermal cycle.

The main conclusions of the present research are: (a) diluted aluminium induces the formation of nanocrystals in a-Ge:H films deposited onto crystalline Si substrates at 220 °C, (b) the absence of hydrogen inhibits the formation of Ge crystallites at low temperatures, (c) Al-doped a-Ge:H (and H-free a-Ge) films deposited onto glass substrates do not crystallize at low temperatures, (d) the thermal annealing of the samples at temperatures $T_A \geqslant 500$ °C provokes the appearance of a crystalline phase, (e) the crystalline fraction of samples where low-T MIC occurs is mono-disperse, i.e., it is dominated by a very narrow distribution of crystallite sizes, which increases with increasing T_A, and (f) at $T_A \geqslant 500$ °C the crystalline phase of the films becomes poly-disperse, with the appearance of a broad distribution of small-size crystallites.

The paper is organized as follows. Section 2 describes the preparation conditions of the samples. The results on crystallization, as deduced from Raman spectroscopy, are presented in section 3 for as-deposited and for thermally annealed samples. Section 4 is divided into five subsections. We discuss first the role of aluminium impurity in the low-T MIC phenomenon, followed by the likely role of hydrogenation in the whole process. The mechanical properties of the samples and the importance of compressive stress are discussed next, followed by a discussion on the role of the substrate on the appearance of crystal seeds. Finally, the analysis of the crystallite size distribution under different preparation conditions and annealing temperatures conclude section 4. Section 5 summarizes the main findings of the work.

2. Experimental details

Electronic quality a-Ge:H(Al) samples were deposited onto polished (air-exposed) crystalline silicon ⟨111⟩ and onto Corning 7059 glass substrates kept at $T_D = 220$ °C in a high-vacuum radio frequency (RF) sputtering system using argon as a sputtering gas [8]. All depositions employed a 3 inch diameter crystalline pure Ge target, the deposition rate being typically 1 Å s^{-1}. The doping of a-Ge films was achieved by partially covering the c-Ge target with small pieces of Al metal. The metal concentration in the samples was determined with the proton-induced x-ray emission technique (PIXE). The present research considers four series of samples: A, B, C, and D. They correspond to: a-Ge:H(Al)/c-Si; a-Ge(Al)/c-Si; a-Ge:H(Al)/glass; and a-Ge(Al)/glass, respectively. Hydrogenated samples, of typical thickness 10^{-4} cm, resulted from the addition of ultra-high purity H_2 to the chamber. H-free samples, deposited under identical nominal conditions, except for hydrogenation, were around 3×10^{-4} cm thick.

The dynamics of the crystallization process was investigated by means of isochronal (15 min) cumulative thermal annealing treatments at 300, 350, 400, 450, 500 and 550 °C, in a temperature-controlled resistive furnace under a continuous flow of argon. Some samples were also annealed at 600 °C. By choosing thermal annealing cycles of 15 min, the present

Table 1. Representative samples of the four series of a-Ge films deposited onto crystalline Si and 7059 glass substrates. The table shows the relative impurity concentration [Al/Ge] and hydrogenation [H] in as-deposited samples. The crystallization path and the crystalline fraction after thermal annealing at 500 and 550 °C are also indicated.

					ρ_C (%)	
Sample	Substrate	[Al/Ge]	[H] (at.%)	Crystallization path	$T_A = 500$ °C	$T_A = 550$ °C
A.1		0	5.7 ± 1.0	Explosive at 500 °C	75	82
A.2	c-Si	5.0×10^{-5}	4.3 ± 1.0	Gradual from 220 °C	52	78
A.3	⟨111⟩	4.5×10^{-4}	4.0 ± 1.0	Gradual from 220 °C	24	72
A.4		2.0×10^{-3}	4.5 ± 1.0	Explosive at 500 °C	56	67
B.1		0	0	Explosive at 550 °C	0	75
B.2	c-Si	1.6×10^{-4}	0	Explosive at 500 °C	85	87
B.3	⟨111⟩	4.8×10^{-4}	0	Explosive at 500 °C	73	76
B.4		1.6×10^{-3}	0	Explosive at 500 °C	84	87
C.1		0	5.7 ± 1.0	Explosive at 550 °C	0	81
C.2	7059	5.0×10^{-5}	4.3 ± 1.0	Amorphous at 550 °C	0	0
C.3	glass	4.5×10^{-4}	4.0 ± 1.0	Explosive at 500 °C	69	76
C.4		2.0×10^{-3}	4.5 ± 1.0	Partial cryst. at 550 °C	0	20
D.1		0	0	Explosive at 500 °C	66	80
D.2	7059	1.6×10^{-4}	0	Explosive at 550 °C	22	80
D.3	glass	4.8×10^{-4}	0	Explosive at 500 °C	92	93
D.4		1.6×10^{-3}	0	Explosive at 500 °C	69	73

contribution explores only the initial steps leading to crystallization. As a consequence, it is not the intention here to compare the present results with those found by other researchers on films deposited under different conditions, or annealed for longer periods of time.

Raman spectra were measured in the backscattering geometry with the 632.8 nm wavelength line of a He–Ne laser. In order to avoid non-intentional crystallization and/or thermal effects, great care was taken with the laser power during the measurements. The Raman signal of both the amorphous and the crystalline phase was fitted using Lorentzian distribution curves. The experimental data were fitted in the 250–325 cm^{-1} frequency range, which considers just the transverse-optical- (TO-) like region of amorphous and crystalline Ge. The crystalline fraction (ρ_C) of the samples, and its evolution with annealing temperature, has been estimated from the integrated areas of the Lorentzian curves used to fit the Raman spectra:

$$\rho_C = \frac{A_C}{A_C + \sigma_R A_A} \tag{1}$$

where A_C and A_A stand for the integrated areas of the crystalline and amorphous phases, respectively; and σ_R (=0.8) is a photon correction factor that takes into account differences between the backscattering cross section of the crystalline and of the amorphous phases [9, 10].

3. Results

Table 1 displays the composition and the crystallization path of four samples of each one of the four series. For comparison purposes, samples containing similar concentrations of aluminium were selected. In all series, an Al-free (intrinsic) sample was also added to help in understanding the role of aluminium impurity in the crystallization process. The behaviour of

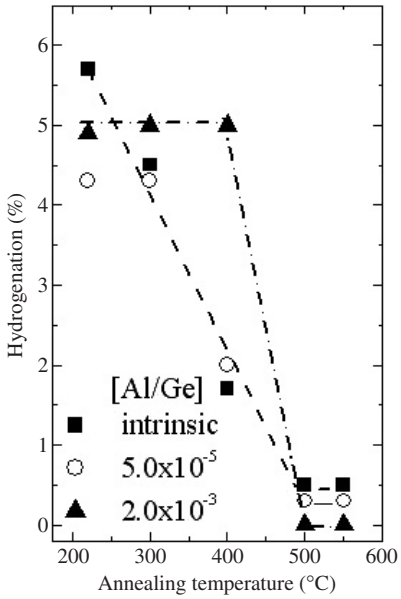

Figure 1. The figure displays the three main trends of hydrogenation as a function of annealing temperature in a-Ge:H(Al)/c-Si samples. In intrinsic samples ([Al/Ge] = 0, filled squares), [H] decreases linearly to an almost zero level at 500 °C. The presence of Al impurity reduces [H] in the samples. At intermediate impurity concentrations, the hydrogenation drops in a way similar to intrinsic samples. At the largest Al concentration [Al/Ge] $\sim 2 \times 10^{-3}$, the hydrogenation remains constant up to $T_A = 400\,^{\circ}C$, an indication of the lack of mobile H in the network. The lines are guides to the eye.

the selected Al-doped samples of each series (see table 1) is representative of the remaining samples of the series. At this point, it is important to emphasize that, purposely, small Al impurity concentrations [Al/Ge] $\leqslant 2 \times 10^{-3}$, i.e., doping range, have been chosen to study the MIC phenomenon. The reason behind the choice of a highly diluted impurity is simply to avoid metal aggregates and/or metal–semiconductor interfaces. In other words, we address the MIC phenomenon under conditions far from the Ge–Al alloy phase.

The hydrogen concentration of the a-Ge:H/c-Si films was estimated from the integrated area of the wagging absorption band of the Ge–H dipoles [11]. Since hydrogenated films were deposited simultaneously onto c-Si and onto glass substrates, we assume an identical hydrogen concentration in both cases. Figure 1 shows the evolution of hydrogenation with annealing temperature. Note the different behaviour of hydrogenation of sample D.4, with [Al/Ge] $\sim 2 \times 10^{-3}$.

Under thermal annealing, Al-doped a-Ge:H/c-Si samples crystallize either gradually or in a sudden, or explosive, way [7]. With the exception of samples A.2 and A.3, all the samples shown in table 1 crystallize only at $T_A \geqslant 500\,^{\circ}C$.

Partially crystallized films exhibit a Raman spectrum with two contributions (figure 2). One is a featureless scattering signal, peaking at approximately 275 cm^{-1} with a full width at half maximum (FWHM) of ∼40–50 cm^{-1} that corresponds to the TO-like Raman signal of the amorphous Ge phase. The other scattering signal, of variable intensity, occurs at ∼300 cm^{-1} and originates from relatively large germanium crystallites (average size $\langle L \rangle \geqslant 10$ nm, FWHM ∼5–7 cm^{-1}) embedded in the a-Ge network. The intensity of the scattered signal depends on the crystalline fraction, whereas both the frequency and FWHM are associated with the crystallite size and with the existence of stress.

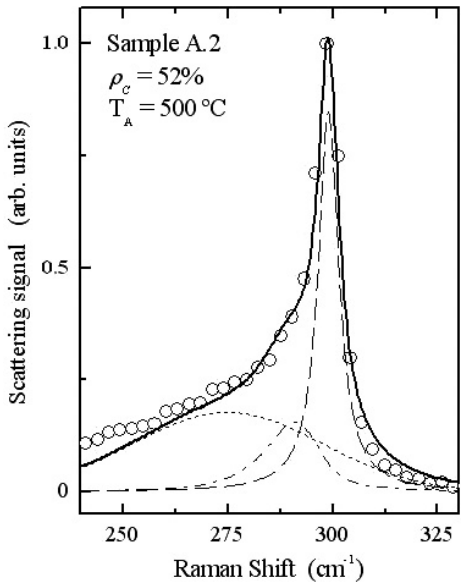

Figure 2. Raman spectrum of sample A.2 after a thermal treatment at 500 °C. A good fit to the experimental data (open circles) requires three Lorentzian curves, as shown in the figure. The broad curve (dotted line) centred at 275 cm^{-1} originates from the amorphous Ge phase. The narrow dashed line, peaking at ∼300 cm^{-1}, is the contribution of relatively large Ge crystallites, whereas the third Lorentzian (dash–dot) originates from Ge crystallites of small size.

As expected, the signal of the crystalline phase becomes dominant as the annealing temperature increases. In some cases, particularly at $T_A \geqslant 500\,°C$, the Raman signal corresponding to the crystalline phase widens and becomes asymmetric. To obtain a reasonable fit to the measured spectra a third contribution is required, as shown in figure 2. In the present research, this extra Lorentzian distribution curve has been interpreted as stemming from the existence of small-size crystallites ($\langle L\rangle \leqslant 8$ nm) [6, 12]. As shown in what follows, the crystallization process induced by the aluminium impurity is dominated at low T by a very narrow distribution of crystallite sizes, an indication of a mono-disperse system. As T_A increases, however, the crystallite size distribution includes nanocrystals of smaller size, indicating a poly-disperse system. The experimental results suggest a thermal origin for the small-size crystallites.

Although Raman spectroscopy is a suitable tool to study crystallization processes [13], it is unable to detect crystallites of size smaller than ∼10–20 Å, i.e., the technique is not powerful enough to identify the very initial steps of atomic ordering around a crystal embryo.

A summary of the crystallization process of each of the series is presented below.

Series A. The analysis of the Raman spectra of the a-Ge:H(Al)/c-Si samples indicates the existence of some spontaneous crystallization at $T_D = 220\,°C$. The low-T crystallization of the a-Ge:H/c-Si films induced by minute amounts of aluminium impurity [$10^{-6} <$ [Al/Ge] $< 10^{-3}$], as well as the lack of any detectable low-T crystallization in sample A.4, have been discussed in detail in [7]. Most of these effects originate from the way hydrogen bonds to the Ge network in the presence of an increasing concentration of Al. Note that Al-free films do not crystallize at low T.

Series B. The Raman spectra of H-free a-Ge(Al)/c-Si samples indicate that the inclusion of aluminium impurity in films deposited onto crystalline silicon substrates is not sufficient

to induce their low-T crystallization (see table 1). This experimental finding indicates that hydrogen plays a fundamental role in the low-T MIC process under study. In other words, aluminium atoms appear to be the active crystallization seed only in hydrogenated a-Ge(Al) films.

Series C. The series corresponds to hydrogenated a-Ge:H(Al)/glass samples deposited in the same deposition run as those of series A, which display a low-T MIC behaviour. The Raman spectra of the as-deposited and of the annealed series C samples indicate that: (a) Sample C.1 (Al-free hydrogenated a-Ge) crystallizes explosively at $T_A = 550\,^{\circ}C$. (b) Sample C.2, with [Al/Ge] $\sim 5 \times 10^{-5}$ remains amorphous up to $T_A = 550\,^{\circ}C$. (c) Sample C.3 crystallizes explosively at $T_A = 500\,^{\circ}C$. (d) Sample C.4 ([Al/Ge] $\sim 2 \times 10^{-3}$) remains partially crystallized at $T_A = 550\,^{\circ}C$. In summary, there is no low-T partial crystallization on a-Ge:H(Al) samples deposited onto glass, a clear indication that the nature of the substrate influences the crystallization process.

Series D. The H-free Al-doped a-Ge films deposited onto glass of series D do not display any low-T MIC. Note, however, that all films of series D display a considerable crystalline fraction at 500 °C. Moreover, the crystalline fraction of series D films at 550 °C is the largest of all series. The comparison between the crystallization path of samples of series C and D indicates that the presence of hydrogen hinders the crystallization of Al-doped a-Ge samples deposited onto glass.

It is clear from the above considerations that diluted aluminium impurity induces the low-T partial crystallization of a-Ge films under special circumstances only. The results highlight the roles of aluminium impurity and of hydrogenation, as well as the importance of the nature of the substrate.

4. Discussion

4.1. The role of aluminium impurity

The effect of aluminium impurity on the MIC of hydrogenated a-Ge films deposited onto c-Si has been considered in detail in [7]. Let us briefly recall the main results. Boron, aluminium, gallium, and indium impurities act as p-type doping elements in a-Ge:H. Studies by extended x-ray absorption fine structure (EXAFS) [14] on the coordination of and on the local order around Ga impurity in a-Ge:H indicate that the impurity keeps the fourfold coordination of the host up to an impurity relative concentration [Ga/Ge] $\sim 0.1\%$, the incorporation of diluted Ga causing a local distortion of the network. The valence structure and the size of the electron cloud radius in the tetrahedral coordination ($\sim$1.26 Å) are the same for Al and Ga [15]. The experimental EXAFS data on samples containing increasing amounts of Ga show that, as [Ga/Ge] increases, the Ga–Ge first-shell distance decreases and the short-range order around the impurity improves, the effect stemming from the additional internal stress provoked by Ga_4 in the network.

In a crystalline network the large (negative) energy difference between the fourfold substitutional (Ga_4) and the strongly distorted threefold (Ga_3) impurity configurations sets practically all impurities in the doping Ga_4 configuration. In an amorphous network, a competition between the sp^3 promotional energy cost for the formation of Ga_4 and the deformation energy for the formation of Ga_3 occurs, which locally determines the preferred impurity coordination. In a real amorphous semiconductor, as opposed to a continuous random network (CRN), one may expect the existence of medium-range order (MRO), as indeed observed in as-grown a-Ge films by variable coherence transmission electron microscopy (VCTEM) [16]. This result suggests that the MRO plays a decisive role in the energetic balance

by favouring the Ga_4 coordination through an increase of the deformation energy associated with the competing Ga_3 configuration.

Based on the similarity between Ga and Al, a plausible phenomenological explanation of the role played by Al in the low-T crystallization of a-Ge indicates that diluted Al atoms (as Ga atoms) remain essentially fourfold coordinated (Al_4) up to a relative concentration [Al/Ge] $\sim$ 0.1%. The compressive field induced by Al_4 and Al_4^- impurities is enhanced by the presence of hydrogen in the network. The experimental findings on Ga impurity lead us to consider that the low-temperature crystallization induced by aluminium results in fact from the combination of an improved order around Al_4 and an augmented compressive stress. The improved order around the metal impurity and the shrinkage of the first metal–semiconductor shell distance, as measured on Ga impurity, should be enhanced in the case of Al. The absence of d electrons in Al results in a stiffer sp^3 hybridized orbital—better ordering—and a more compressive electron cloud. Note that, differently from Al, Ga impurity does not induce any low-T crystallization of a-Ge:H. This interpretation is consistent with *ab initio* calculations on relaxed and compressed Ge clusters ($Ge_{58}H_{60}X$), in which the central atom (X) is replaced by a group III impurity [17]. According to the calculations, neutral Al tends to be more tetrahedral than B or Ga. These experimental and theoretical results strongly suggest that in series A samples fourfold-coordinated Al atoms act as crystallization seeds. At this point, it is important to remark that the above considerations fail to explain the absence of any low-T crystallization of series C samples, which are identical to those of series A, but deposited onto glass. As recently observed in the MIC of Ni-containing a-Si films [18], substrates having a periodic surface promote the nucleation of crystal seeds at the film–substrate interface, whereas the disordered surface of amorphous substrates does not favour the appearance of such crystal embryos. We come back to this question in subsection 4.4.

4.2. Thermal annealing, hydrogenation and structural properties

Hydrogen too exerts a great influence on the MIC process of a-Ge films. Hydrogen species not only passivate dangling orbitals, but also allow a more favourable environment to the development of Ge crystallites [7]. Depending on the deposition conditions and final atomic composition, hydrogen species can assume three different bonding configurations in the a-Ge network: (1) H bonded to Ge on the surface of microvoids (bulk-like Ge–H), (2) H atoms on the internal surfaces of larger voids (surface-like Ge–H), and (3) molecular hydrogen. They are sensitive to thermal annealing treatments; hydrogen in the bulk-like configuration diffuses at relatively low temperatures ($\sim$300 °C), whereas surface-like bonded hydrogen leaves the network at $T_A \geqslant 400$ °C.

A-Ge:H(Al)/c-Si samples containing $10^{-6} <$ [Al/Ge] $< 10^{-3}$ crystallize partially at $T_D = 220$ °C and start losing bulk-like Ge–H bonds at $T_A > 300$ °C. At $T_A \sim 400$ °C the most mobile hydrogen has been lost by the network. This is not the case for sample A.4, in which changes in hydrogenation—as measured by infrared spectroscopy—only appear at $T_A > 400$ °C. According to experimental data [7], an increasing concentration of aluminium in the network reduces the amount of bulk-like Ge–H bonds. The absence of mobile hydrogen in sample A.4 seems to originate from an increased aluminium concentration, which prevents the partial crystallization at temperatures smaller than 500 °C. The data suggest that, at low T, mobile hydrogen in the a-Ge network allows creating the highly disordered regions that connect randomly oriented crystallites. The picture is consistent with the absence of any low-T partial crystallization of H-free samples (series B and D). Again, the MIC process depends on the nature of the substrate.

4.3. Mechanical stress

It is well known that compressive stress induces the crystallization of thin amorphous films [19]. The stress in amorphous semiconductor films arises from different causes [20]: stress during the deposition process (intrinsic stress), stress after cooling–heating cycles (thermal stress), and stress due to differences between the film and the substrate (interfacial stress). The film composition (presence of impurities and/or of embedded gaseous species) also contributes to the intrinsic stress.

A detailed study of the thermo-mechanical properties of RF-sputtered a-Ge:H films deposited under conditions similar to the films of the present contribution has been reported by De Lima Jr *et al* [21]. These authors determined the internal mechanical stress of 1–3 μm thick films deposited onto four different substrates: Si $\langle 111 \rangle$, Ge $\langle 111 \rangle$, 7059 Corning glass, and quartz. Their study considers the influence of hydrogenation and of annealing temperature on stress. It was found that: (a) RF-sputtered a-Ge:H films of good electronic quality are always compressively stressed, (b) films deposited onto c-Si substrates and containing 5 to 10 at.% hydrogen display a stress of about 0.5 GPa at room temperature, and (c) the highest compressive stress is measured in films deposited onto glass. For all the substrates the stress in the films increases with thermal annealing, as well as with an increasing hydrogenation. The stress induced by hydrogenation in a-Ge:H films may originate from voids and/or from the presence of molecular hydrogen trapped in the network [22].

Hydrogen, however, is not the only source of stress in a-Ge films. The compressive stress measured in H-free a-Ge films amounts to $\sim$0.25 GPa [23]. The residual stress may be caused by the incorporation of a few per cent of argon atoms in the network, a consequence of the non-bonding properties of noble gases and to the fact that the electron cloud radius of Ar ($\sim$1.87 Å) is much larger than that of the host Ge ($\sim$1.23 Å). Note also that, for the Al-doped a-Ge:H samples of table 1, the aluminium impurity also constitutes an additional source of compressive stress.

Turn *et al* [24] studied the mechanical properties of plasma-enhanced chemical vapour deposited dielectric films onto different substrate materials and concluded that the intrinsic deposition stress is not necessarily the same on two different substrates. The variation of film stress with substrate suggests that the interfacial bonding during the initial stages of deposition propagates to affect the entire film. These authors also found that irreversible stress develops on thermal annealing, one of the main causes being hydrogenation. In the present analyses, we estimated the order of magnitude of the compressive stress provoked by the different thermal expansion coefficient (TEC) between film and substrate as a function of annealing temperature, hydrogenation, and the thickness of the substrate. For such a purpose, we used the modified Stoney equation for thin films [25] and the biaxial modulus and the TEC of the substrate materials measured at different temperatures. The main results of the calculations are as follows.

(1) During thermal annealing cycles the compressive stress originating from a different TEC between film and substrate is always a minor fraction of the intrinsic stress of the film (10% at the most). This additional compressive stress alone is not sufficient to induce the low-T crystallization of a-Ge.
(2) Hydrogenated samples deposited onto glass substrates are the most compressively stressed, in agreement with the measurements of [21].

Summarizing, the data of table 1 indicate that the compressive stress originating from hydrogenation, impurities, and/or other network defects does not, by itself, provoke the crystallization of a-Ge at low temperatures. In contrast, the results shown in table 1 indicate

that only the combined effects of hydrogenation, aluminium impurity, and the crystalline nature of the substrate trigger the low-T MIC phenomenon. None of them induces separately the appearance of Ge crystallites at $T_A < 500\,^{\circ}C$.

4.4. The role of the substrate

We consider now the influence of the substrate on crystal seed formation at low T. The crystallization of an amorphous film may be influenced by the substrate in several ways: (a) the physical structure of the surface onto which the film is deposited; (b) its roughness and/or crystalline character; (c) the crystal orientation; (d) the presence of oxide layers or contaminants, etc.

The nucleation and growth by solid-phase epitaxy of the first monolayers of germanium onto clean silicon surfaces has been the subject of research of several groups [26–29]. The relatively large lattice mismatch (4.2%) between the two lattices provokes an important strain in the initial Ge layers, which is relaxed through a clustering mechanism. Despite the important differences between molecular beam epitaxy and RF sputtering, the present experimental results indicate that, depending on the simultaneous presence of aluminium impurity and hydrogen, the formation of ordered Ge clusters—possibly around Al_4 atoms—is induced onto the c-Si surface during the deposition of the initial Ge layers, any remaining strain being relieved by mobile H bonding. Although a detailed knowledge of interfacial bonding between film and substrate and its propagation during growth is not available, the results suggest that, as the deposition process proceeds, the interfacial crystalline embryos propagate in the growth direction along the entire film thickness. This being the case, the density of interfacial crystal seeds should increase with an increasing metal concentration, as detected for highly diluted doping. Under these circumstances, the effect of thermal annealing at increasing temperatures would be to increase the dimensions of the crystallites. The analysis of the crystal size variation with T_A in series A samples, where Al-induced low-T MIC occurs, strongly supports this phenomenological description. In other words, at low temperatures, crystalline Ge seeds are formed at the film–c-Si interface and not in the bulk of the film. The absence of any low-T MIC in identical samples deposited onto glass is consistent with the picture. Hence, the Al-induced nanocrystal nucleation process requires the presence of a periodic (crystalline) surface, aluminium impurity, which acts as a seed, and mobile hydrogen that helps in relaxing the strain originating from lattice mismatch. As said, the absence of any one of these components prevents the appearance of Ge crystal seeds at low T. The picture agrees with the experimental findings on crystallization in the remaining three series (B, C, and D), in which the crystallization of a-Ge only occurs at high temperatures, i.e., $T_A \geqslant 500\,^{\circ}C$.

4.5. Crystallite size distribution

Because of phonon confinement effects in small crystals, the first-order Raman scattering signal becomes broader and the peak frequency shifts toward small frequencies as the crystal size diminishes [30]. The theoretical Raman scattering intensity $I(\omega)$ given by small spherical crystallites, found in good agreement with experimental data [31, 32], reads

$$I(\omega) = \int \frac{|C(0,\vec{q})|^2}{[\omega - \omega(\vec{q})]^2 + (\Gamma_0/2)^2}\, \mathrm{d}^3\vec{q} \tag{2}$$

where $\omega(\vec{q})$ is the phonon dispersion relation, Γ_0 is the bandwidth (FWHM) of the scattered signal, and $C(0,\vec{q})$ is the Fourier transform of the phonon confinement, its value depending on the crystallite size L. As only the phonons near the zone centre contribute to the scattering signal, the integration of equation (2) is done assuming a spherical Brillouin zone and using the

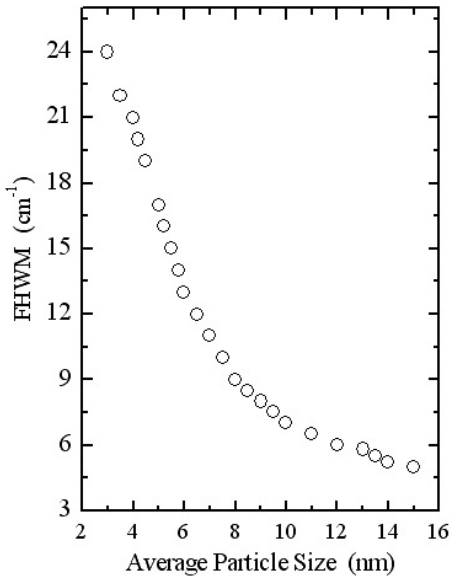

Figure 3. Open circles: full width at half maximum (FWHM) of the Raman scattering signal given by small spherical nanocrystals as a function their size. These data have been used to estimate the size distribution of crystallites embedded in the Ge amorphous network.

confinement function given by Campbell and Fauchet [30]. The solution is a Lorentzian curve, the position and the width of which depend on the crystallite size.

$$I(\omega) = \frac{2A}{\pi} \frac{\Gamma_0}{4(\omega - \omega_0)^2 + \Gamma_0^2}. \tag{3}$$

Figure 3 shows the average crystallite size $\langle L \rangle$ as a function of the FWHM of the Raman signal. Note that the presence of a compressive stress in the films—as is the case of the present samples—induces an opposite behaviour to the red shift of the Raman peak as the crystal size decreases, i.e., under pressure the peak of the scattered signal shifts to higher frequencies [33]. To circumvent the difficulty, the FWHMs of the Lorentzian distributions fitting the Raman spectra were considered to find the average crystallite size, as deduced from figure 3.

The dominant crystalline contribution peaking at ∼300 cm^{-1} (FWHM ∼6–7 cm^{-1}) corresponds to Ge crystallites of 10–11 nm average size. The second Lorentzian that may be necessary to obtain a good fit to the crystalline phase of the experimental spectra is broader than the main peak. It can be decomposed into a series of smaller contributions, the sum of which reproduces the single curve fit. The method enables a better fitting and gives indications of the distribution of crystallite sizes in the film. In the process of building the crystal size distribution, the relation between FWHM and average crystal size given in figure 3 has been obeyed in all cases.

Different numerical experiments were done to test the validity of the assumption. The tests consisted in calculating the theoretical Raman scattering signal given by a known distribution of nanocrystal sizes embedded in an amorphous matrix. The calculated Raman signal was then inverted to retrieve the crystal size distribution from which the scattering signal was generated. The numerical experiments done with distributions of crystallites of several sizes were always successful, in the sense that the original distribution was always retrieved (see figure 4). The advantage of testing the method with computer-generated crystal size distributions is that the

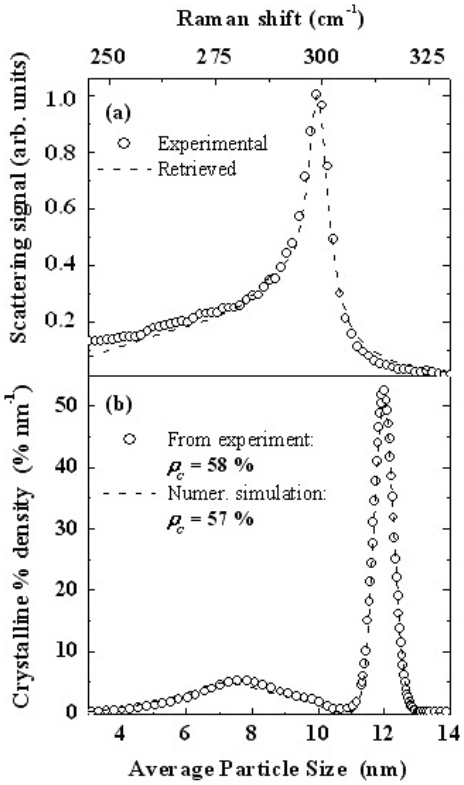

Figure 4. (a) Measured Raman spectrum (open circles) and numerically retrieved scattering signal (dashed line) calculated from the distribution of crystal sizes given below. (b) Comparison of the crystal size distribution estimated from the fit to the experimental Raman spectrum (open circles) and the distribution (dashed line) used to generate the theoretical Raman spectrum shown in (a). A good agreement between numerical experiment and measured data has been found in all cases.

true response is known in advance and both the goodness and the limitations of the retrieval can be readily tested. The retrieval method was systematically applied to experimental Raman spectra to estimate the crystal size distribution after each thermal cycle. A spherical shape crystallite was adopted in the retrieval process because the penetration depth of the laser radiation in the material is similar to the crystallite sizes under consideration.

As an example, consider figure 5, which shows the evolution of the nanocrystal size distribution of sample A.2 after annealing cycles at increasing temperatures (see table 1 and figure 2). Let us remember that A.2 is an a-Ge:H(Al)/c-Si sample that presents the low-T MIC phenomenon. Figure 5 displays the size distribution of Ge nanocrystals as a function of T_A, and the crystalline fraction after each thermal treatment. We remark that the as-deposited sample is already 22% crystalline (see figure 5). It is interesting to analyse the evolution of the Ge nanocrystal size as the sample is being annealed. At $T_D = 220\,^{\circ}$C the crystalline phase is mono-disperse and dominated by nanocrystals of small size; i.e., 9 nm diameter. As the annealing process progresses, the size of the dominant nanocrystal increases: 10 nm at 300 °C; 11 nm at 400 °C; 12 nm at 500 °C; attaining 15 nm at $T_A = 550\,^{\circ}$C. Another interesting experimental finding is that, for $T_A \geqslant 500\,^{\circ}$C (figure 5, open circles), a broad distribution of small crystals appears, peaking at $\langle L \rangle \sim 7.5$ nm. In other words, at $T_A \geqslant 500\,^{\circ}$C the crystalline phase becomes poly-disperse. At $T_A = 550\,^{\circ}$C (filled circles in figure 5) the broad

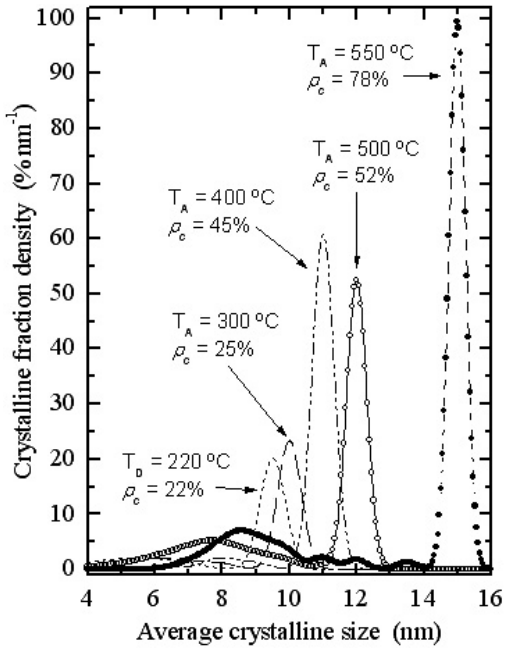

Figure 5. Evolution of the crystal size distribution and of the crystalline fraction ρ_C of sample A.2 (a-Ge:H(Al)/c-Si; [Al/Ge] $\sim 5 \times 10^{-5}$) as a function of the annealing temperature. Note that the size of the main crystallite increases at increasing T_A. At $T_A \geqslant 500\,^{\circ}$C the fitting of the Raman spectra requires the inclusion of a distribution of small-size crystallites ($\langle L \rangle \sim 8$ nm). Also note that at $T_A = 550\,^{\circ}$C an important increase of both the size of the main crystallite and the crystalline fraction occurs.

distribution of small crystallites peaks at 8.5 nm. Note that $T_A = 500\,^{\circ}$C is the temperature at which Al-free a-Ge films crystallize, suggesting that the broad distribution of small-size nanocrystals does not originate from the presence of the metal impurity. This pattern is identical in all the samples showing the low-T MIC phenomenon. The picture can be explained as follows. During the very first steps of film deposition, crystal seeds are formed around Al_4 atoms at the film–c-Si substrate interface. As the film grows, the crystal Ge embryos propagate in the growing direction. The density of nanocrystal seeds does not change with increasing T_A up to a temperature when thermal crystallization occurs. The increased crystal size and crystalline fraction measured with increasing annealing temperatures is the consequence of the thickening of the already existing crystal seeds, the crystalline phase being of a mono-disperse nature. In other words, as T_A increases more neighbouring Ge atoms incorporate to the existing nanocrystals. The process continues and becomes more effective as $T_A \geqslant 500\,^{\circ}$C, but at these high temperatures the remaining amorphous tissue crystallizes spontaneously, giving rise to a large density of smaller crystallites.

The above phenomenological picture is consistent with the data giving the crystalline fraction ρ_C of a-Ge:H(Al)/c-Si samples as a function of Al concentration at different annealing temperatures, as displayed in figures 6 and 7.

Figure 6 shows the following. (a) Aluminium impurity enhances the crystallization mechanism. (b) At $T_D = 220\,^{\circ}$C, ρ_C increases as the [Al/Ge] fraction increases up to a maximum of about 20% at [Al/Ge] $\sim 10^{-4}$. (c) The crystalline fraction does not change appreciably between $T_D = 220\,^{\circ}$C and $T_A = 300\,^{\circ}$C and remains almost constant ($\rho_C \sim 20\%$)

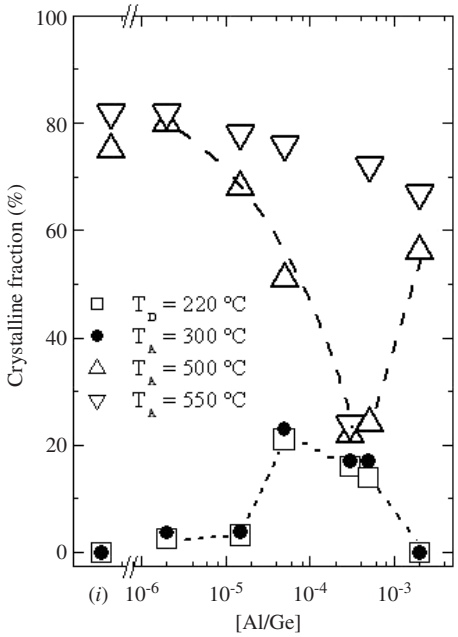

Figure 6. Crystalline fraction versus relative aluminium concentration at different annealing temperatures for series A samples; i.e., a-Ge:H(Al)/c-Si films. Note the different crystalline fraction at $T_D = 220\,^{\circ}\mathrm{C}$ and at $T_A = 500\,^{\circ}\mathrm{C}$ as a function of aluminium concentration. The lines are guides to the eye.

for [Al/Ge] between 5×10^{-5} and 5×10^{-4}. (d) In this [Al/Ge] concentration range, the overall crystalline fraction of the samples at $T_A = 500\,^{\circ}\mathrm{C}$ decreases. The likely reason is an increasing density of Al_3 sites in the amorphous tissue connecting the crystallites, a consequence of the increasing interaction of Al and hydrogen, which promotes Al_3 bonding configurations. At high temperatures, once mobile hydrogen atoms have left the network, the network configuration containing Al_3 sites does not favour the crystallization of Ge. (e) In samples containing little or no mobile hydrogen at all, the crystalline fraction at $T_A = 500\,^{\circ}\mathrm{C}$ is relatively large, in accordance with the previous interpretation. (f) When [Al/Ge] $\sim 10^{-3}$ there is no longer any MIC phenomenon. The spontaneous partial crystallization at low T does not occur in the [Al/Ge] 10^{-3}–10^{-2} range, as reported in [6, 7]. (g) In all cases, the crystalline fraction at $T_A \geqslant 550\,^{\circ}\mathrm{C}$ increases again. However, the presence of aluminium in the a-Ge network still inhibits the complete crystallization at elevated temperatures ($T_A \geqslant 550\,^{\circ}\mathrm{C}$).

Figure 7 shows the above-mentioned trends, but in a different representation. The following are apparent from figure 7. (a) The crystalline fraction ρ_C at $T_D = 220\,^{\circ}\mathrm{C}$ increases at first with increasing aluminium concentration, the maximum $\rho_C \sim 20\%$ corresponding to [Al/Ge] $\sim 10^{-4}$. A relative Al concentration larger than 10^{-4} provokes a reduction of ρ_C at $T_D = 220\,^{\circ}\mathrm{C}$, any detectable crystallization disappearing for [Al/Ge] $\sim 2 \times 10^{-3}$. (b) The variation of the crystalline fraction with annealing temperature also depends on the relative metal impurity content: the larger the spontaneous crystallization at T_D the larger the increase of the crystalline fraction at increasing T_A. Both effects are related to the concentration of mobile hydrogen and of aluminium, as explained.

Regarding the a-Ge films deposited onto glass substrates, table 1 shows that they do not present any low-T MIC. The data indicate that the presence of hydrogen inhibits the

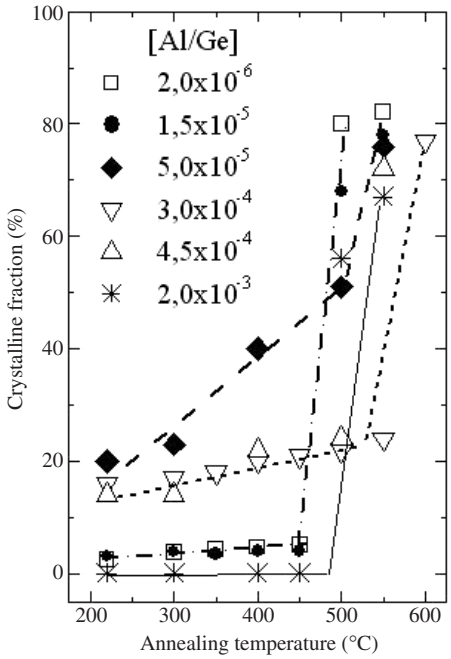

Figure 7. Crystalline fraction of a-Ge:H(Al)/c-Si samples having different [Al/Ge] impurity concentrations as a function of annealing temperature. Note that, at first, the low-T MIC fraction increases with increasing Al concentration and, then, decreases to zero for [Al/Ge] $\sim 2 \times 10^{-3}$. See text. The lines are guides to the eye.

crystallization of a-Ge, most probably via a not yet studied hydrogen–oxygen reaction. As shown in figure 8, the explosive crystallization occurring at elevated temperatures indicates nanocrystals of, typically, 10–12 nm diameter. In most cases, a broad distribution of small crystallites is also present.

5. Conclusions

This contribution addresses the problem of the Ge nanocrystal formation induced by highly diluted aluminium impurity in an amorphous Ge network. It has been found that, under specific circumstances, a partial crystallization process may occur at temperatures of the order of 200 °C. Samples containing variable, though small, amounts of Al were deposited onto glass and crystalline silicon substrates. The crystallization of the samples is influenced not only by the metal impurity, but also by the presence of mobile hydrogen. Also, it has been found that the low-temperature nanocrystal formation only occurs in a-Ge:H(Al) films when they are deposited onto polished crystalline silicon substrates. The spontaneous formation of crystal seeds appears when the relative metal concentration stays between 10^{-6} and 10^{-3}, i.e., an impurity doping range. The evolution of crystallization with annealing temperature and the analysis of the distribution of crystallite size after thermal annealing suggest that the formation of crystal seeds occurs at the amorphous film–substrate interface. The role that a periodic surface plays in the process, as well as the importance of fourfold-coordinated aluminium as an embryo precursor of Ge nanocrystals, has been discussed. Mobile hydrogen plays a fundamental role in enabling the relaxation of the amorphous tissue surrounding the crystal

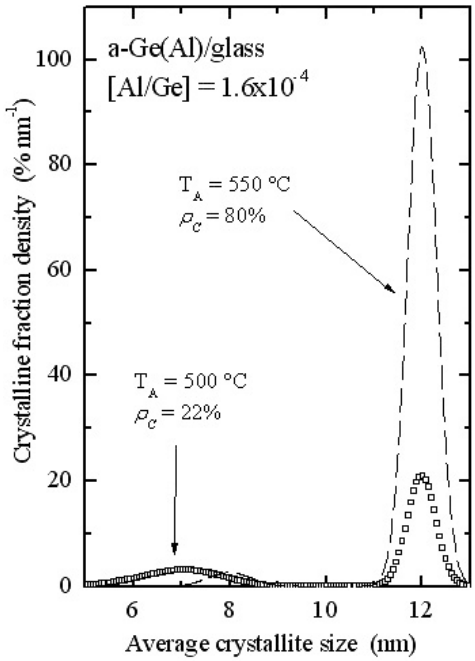

Figure 8. Average crystallite size distribution of sample D.2. Note the distribution of small-size crystallites at $T_A = 500\,^{\circ}C$ centred at about 7 nm. At $T_A = 550\,^{\circ}C$ both the crystalline fraction and the contribution of the large crystallite increase abruptly, the contribution of small-size crystallites becoming negligible.

seed. When all the above-mentioned conditions are not met no low-T crystallization occurs and the amorphous nature of the films disappears only at $T_A \geqslant 500\,^{\circ}C$. The compressive stress present in as-deposited and in thermally annealed samples is not enough to induce the crystallization of a-Ge thin films in any substrate.

The experimental data presented here confirm that the metal-induced crystallization of amorphous semiconductors may be triggered at an atomic level and does not require the existence of metal–semiconductor interfaces. The present results may find some useful application in the manufacturing of low-temperature electronic devices.

Acknowledgments

This research has been partially supported by the Brazilian agencies FAPESP and CNPq.

References

[1] Oki F, Ogawa Y and Fuyiki Y 1969 *Japan. J. Appl. Phys.* **8** 1056
[2] Herd S R, Chaudhari P and Brodsky M H 1972 *J. Non-Cryst. Solids* **7** 309
[3] Chalamala B A and Temple D 2005 *IEEE Spectr.* **44** (September)
[4] Hu S M 1991 *J. Appl. Phys.* **70** R53
[5] Chambouleyron I, Fajardo F and Zanatta A R 2001 *Appl. Phys. Lett.* **79** 3233
[6] Chambouleyron I, Fajardo F and Zanatta A R 2002 *J. Non-Cryst. Solids* **299–302** 143
[7] Zanatta A R and Chambouleyron I 2005 *J. Appl. Phys.* **97** 094914

[8] For details see, Marques F C and Chambouleyron I 1989 *9th E.C. Photovoltaic Solar Energy Conf.* ed W Paltz, G T Wrixon and P Helm (Dordrecht: Kluwer–Academic) p 1042
[9] Tsu R, Gonzalez-Hernandez J, Chao S S, Lee S C and Tanaka K 1982 *Appl. Phys. Lett.* **40** 534
[10] Fujii M, Hayashi S and Yamamoto K 1991 *Japan. J. Appl. Phys.* **30** 687
[11] Fang C J, Grutz K L, Ley L, Cardona M, Demond F J, Muller G and Kalbitzer S 1982 *J. Non-Cryst. Solids* **35/36** 255
[12] Iqbal Z, Veprek S, Webb A P and Capezzuto P 1981 *Solid State Commun.* **37** 993
[13] Dos Santos D R and Torriani I L 1993 *Solid State Commun.* **85** 307
[14] Chambouleyron I, Comedi D, Dalba G, Fornasini P, Grisenti R and Rocca F 2000 *Solid State Commun.* **115** 89
[15] Pauling L 1960 *The Nature of the Chemical Bond* 3rd edn (New York: Cornell University Press)
[16] Gibson J M and Treacy M M J 1997 *Phys. Rev. Lett.* **78** 1074
[17] Gozzo F 2004 private communication
[18] Ferri F A, Zanatta A R and Chambouleyron I 2006 *J. Appl. Phys.* **100** 094311
[19] Hekmatshoar B, Shahrjerdi D, Mohajerzadeh S, Khakifirooz A, Goodarzi A and Robertson M 2003 *J. Vac. Sci. Technol.* A **21** 752
[20] Campbell D S 1970 *Handbook of Thin Film Technology—Mechanical Properties of Thin Films* (New York: McGraw-Hill) chapter 12
[21] De Lima M M Jr, Lacerda R G, Vilcarromero J and Marques F C 1999 *J. Appl. Phys.* **86** 4936
[22] Marques F C, Wickboldt P, Pang D, Chen J H and Paul W 1998 *J. Appl. Phys.* **84** 3118
[23] De Lima M M Jr and Marques F C 2001 *Thin Solid Films* **398/399** 540
[24] Turn J, Cook R F, Kamarajuggada M, Bozeman S P and Stearns L C 2004 *J. Appl. Phys.* **95** 967
[25] Townsend P H, Barnett D M and Brunner T A 1987 *J. Appl. Phys.* **62** 4438
[26] Osten H J, Klatt J, Lippert G, Dietrich B and Bugiel E 1992 *Phys. Rev. Lett.* **69** 450
[27] Sumitomo K, Nishioka T, Shimizu N, Shinoda Y and Ogino T 1994 *J. Vac. Sci. Technol.* A **13** 289
[28] Suzumura I, Okada M, Muto A, Torige Y, Ikeda H, Sakai A, Zaima S and Yasuda Y 2000 *Thin Solid Films* **369** 116
[29] Zhang Y P, Yan L, Xie S S, Pang S J and Gao H J 2001 *Appl. Phys. Lett.* **79** 3317
[30] Campbell I H and Fauchet P M 1986 *Solid State Commun.* **58** 739
[31] Nemanich R J, Solin S A and Martin R M 1981 *Phys. Rev.* B **23** 6348
[32] Richter H, Wang Z P and Ley L 1981 *Solid State Commun.* **39** 625
[33] Anastassakis E, Pinczuk A, Burstein E, Pollak F H and Cardona M 1970 *Solid State Commun.* **8** 133